

Temperature Effect on the Synthesis of Au–Pt Bimetallic Nanoparticles

Domingo I. Garcia-Gutierrez,[†] Claudia E. Gutierrez-Wing,^{†,‡} Lisandro Giovanetti,[§] José M. Ramallo-López,[§] Félix G. Requejo,[§] and Miguel Jose-Yacamán^{*,†,||}

The Texas Materials Institute, The University of Texas at Austin, 1 University Station C2201, Building ETC, Room 8.102, Austin, Texas 78712-1063, Instituto Nacional de Investigaciones Nucleares, Carr. México-Toluca Km 36.5, Ocoyoacac, Edo. de México 52045, Mexico, Department of Chemical Engineering, The University of Texas at Austin, 1 University Station C0400, Austin, Texas 78712-1062, and Departamento Física, FCE, UNLP and IFLP-INIFTA (CONICET), CC67-CP 1900 La Plata, Argentina

Received: April 30, 2004; In Final Form: November 19, 2004

Pt–Au bimetallic nanoparticles have been synthesized by the polyol method and stabilized with poly(vinylpyrrolidone) (PVP), modifying the temperature of synthesis. Interesting structure changes were observed in the nanoparticles as the temperature was varied. At lower temperatures no bimetallic nanoparticles were detected, but as the temperature increased bimetallic nanoparticles started to appear, commonly obtaining core–shell nanoparticles, always covered by the polymer. This originates the modification of the optical response of the system in the UV–visible region. An absorption peak centered at 520 nm at low temperatures was observed (100–110 °C); at higher temperatures (130–170 °C) there were non detectable absorption peaks, and finally at the two highest temperatures (180–190 °C) the reappearance of an absorption feature centered at 510 nm was noticed. These UV–visible results indirectly imply the composition of the surface of the particle. The structure of the particles has been determined using transmission electron microscopy and high-angle annular dark field (HAADF), the latter being a powerful technique to determine the structural composition of the particles and allowing a direct correlation of the optical response with their structural composition. X-ray absorption near-edge structure (XANES) and extended X-ray absorption fine structure (EXAFS) studies were also performed on the samples and their results support the idea of a Pt_{core}–Au_{shell} structure with the elements segregated from each other. The combination of these experimental techniques with calculated UV–vis absorption spectra allowed, in a reliable way, the elucidation of the nanoparticles structure and elemental distribution.

Introduction

Bimetallic nanoparticles are of great interest because of the modification of properties observed not only due to size effects, but also as a result of the combination of different metals,^{1,2} either as an alloy or as a core–shell structure, modifying the catalytic, electronic, and optical properties of the monometallic nanoparticles.^{1–5}

For this purpose, many colloidal methods of synthesis have been approached to obtain bimetallic nanoparticles,^{6–16} such as homogeneous reduction in aqueous solutions,⁹ or phase transfer reactions,¹⁰ with sodium citrate, hydrazine, NaBH₄, and lithium triethylborohydride (LiBET₃H) as reducing agents, each of them yielding products with different physicochemical and structural characteristics.¹¹ Among these, the polyol method has been reported to produce the core–shell type of nanoparticles as the final product,^{8,12–14} easily changing composition and surface modifiers. This technique does not require an additional reducing agent since the solvent by itself reduces the metallic species.^{15,16} However, besides the stoichiometry and order of addition of reagents in the synthesis process, one of the most important

parameters in the preparation is the temperature. Modifications in temperature influence the reaction by changing the stabilization of the complexes formed between Pt and Au and the surface modifiers, e.g., PVP, and the nucleation rate of the reduced metallic atoms.¹⁷ Characterization of these systems has been a difficult process as stated in previous reports,^{12,18} where researchers have employed indirect measurements to identify the localization of the elements within the nanoparticles. A novel approach to study this kind of particles is based on the use of a high angle annular dark field (HAADF) technique, in a transmission electron microscope (TEM), which allows the observation of the interfaces between layers of different elements due to differences in atomic number, densities, or the presence of strain fields due to differences in lattice parameters.¹⁹ This is mainly useful when the structure of the particles is of the core–shell type. On the other hand, it is known that small metallic particles show characteristic absorption bands in the UV–vis region of the electromagnetic spectrum, but their spectrum can be modified depending on the characteristics of the suspending medium, composition of the metallic structure, the presence of surfactants or any other surface modifier besides the size of the particle.^{3,4,20,21}

This paper reports the effect of temperature on the final nanoparticle characteristics such as size distribution, structure, and stability for the Au–Pt bimetallic system. We analyzed the optical absorption of nanoparticles, the effect of PVP on the

* Corresponding author. E-mail: yacamán@che.utexas.edu.

[†] The Texas Materials Institute, The University of Texas at Austin.

[‡] Instituto Nacional de Investigaciones Nucleares.

[§] UNLP and IFLP-INIFTA.

^{||} Department of Chemical Engineering, The University of Texas at Austin.

surface, the size of the particles, and their core–shell features and related these responses with the nanoparticles structural characteristics as observed by HAADF and as analyzed by X-ray absorption fine structure spectroscopy (XAFS).

Experimental Section

The basic polyol method was followed to obtain mono and bimetallic nanoparticles passivated with poly(vinylpyrrolidone) (PVP). Hydrogen tetrachloroaurate (HAuCl₄) (III) hydrate (99.99%), hexachloroplatinic (IV) acid (H₂PtCl₆) hydrate (99.99%), and poly (N-vinyl-2-pyrrolidone) (PVP–K30, MW = 40000) were purchased from Sigma Aldrich, and 1,2-ethylenediol (99.95%) was purchased from Fischer Chemicals; all the materials were used without any further treatment.

A 0.4 g sample of Poly (N-vinyl-2-pyrrolidone) (PVP) was dissolved in 50 mL of 1,2-ethylenediol (EG) under vigorous stirring, heating in reflux, until the desired temperature was reached (working temperatures ranged from 100 to 190 °C in increments of 10 °C). For the monometallic nanoparticles, a 0.1 mM aqueous solution of the metal precursor was added to the EG-PVP solution, with continuous agitation for 3 h in reflux. When preparing the bimetallic nanoparticles, the following criteria was used: after complete dissolution of PVP in EG, 2 mL of an aqueous solution of H₂PtCl₆ (0.05 M) was added to the EG-PVP solution. One minute after a change in color of the solution from yellow to dark brown was observed, 1 mL of an aqueous solution of HAuCl₄ (0.1 M) was added to the system. The reaction was carried out for 3 h at constant temperature. This order and time between precursors addition was selected after trying several other possibilities. The one chosen for this work presented the smaller nanoparticle average size and smaller standard deviation for a synthesis performed at 140 °C.

For the electron microscopy analysis, samples were prepared over carbon coated copper TEM grids. HAADF images were taken with a JEOL 2010F microscope in the STEM mode, with the use of a HAADF detector with collection angles from 50 mrad to 110 mrad. UV–vis spectra were obtained using a 10 mm path length quartz cuvette in a Cary 5000 equipment. The X-ray absorption spectra were measured at the XAS beamline at the Laboratório Nacional de Luz Síncrotron (LNLS) in Campinas, SP, Brazil. EXAFS and XANES spectra of the Pt L₃-edge (11.56 keV) and L₂-edge (13.27 keV) and Au L₃-edge (11.92 keV) and L₂-edge (13.73) were recorded at 20 K using a Si(220) single channel-cut crystal monochromator in transmission mode and with three ion chambers as detectors (a metal foil was located before the third chamber in order to measure the reference simultaneously with the sample). The Pt monometallic system and the bimetallic system synthesized at 140 °C were analyzed.

Results

Following the polyol method with ethylene glycol as solvent-reductor, it was possible to obtain monometallic and bimetallic nanoparticles with narrow size distributions in systems with small particles (~3 nm) and different structures depending on the temperature of reaction. The monometallic synthesis of nanoparticles by itself showed distinctive morphologies of the nanoparticles depending on the temperature of reaction. As for the bimetallic, it was possible to detect differences in the structures of the nanoparticles, which varied from core–shell nanoparticles to nanoparticles where the metals form eutectic alloys, as it will be discussed later in the text. Also, the size of the bimetallic nanoparticles was modified by the variations in the temperature.

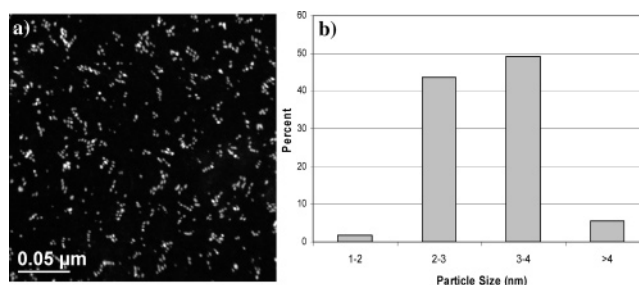
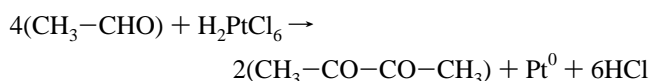
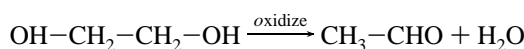
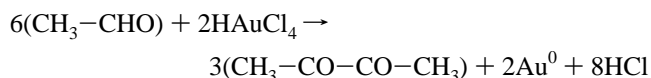
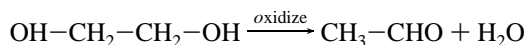


Figure 1. (a) HAADF image of Pt nanoparticles synthesized at 140 °C. Here we can observe a well dispersed sample with a narrow size distribution. (b) Particle size distribution of this sample. The average size observed is 3.11 nm, with a standard deviation of 0.5 nm. The nanoparticles synthesized at 100 and 190 °C showed very similar characteristics.

Reaction proceeds in general as an oxidation of the ethylene glycol reducing the metallic precursor to its zero-valence state^{22,23}



This is the reaction involved in the reduction of Pt⁴⁺ to Pt⁰



This reaction describes the reduction of Au³⁺ to Au⁰.

In the presence of a surface modifier, the reaction changes depending on the ability of the metal to coordinate with it, as in the case of PVP where the metallic precursor could coordinate with the oxygen of the pyrrolidone group, when the particles are in the nanometer size range, while when they are in the micrometer size range the coordination is mainly with the nitrogen, as reported by F. Bonet et al.^{23,24}

Platinum Nanoparticles.

The synthesis of monometallic platinum nanoparticles yielded narrow size distributions centered at 3.11 nm. The temperature in the synthesis of these nanoparticles seemed to not have an important effect on neither the size nor the morphology, as observed by Bonet et al.¹⁶ The Pt particles showed a tendency toward spherical shapes. Figure 1a shows a HAADF image of the particle distribution, and 1b presents the size distribution typical from one sample of this system. It is seen in these images that Pt nanoparticles are very small and have a narrow size distribution, and they remain attached to PVP even after purification of the system, as indicated by the dimensional stability observed by TEM.

Gold Nanoparticles.

In contrast with the type of particles observed in the Pt case, the shape and size of gold nanoparticles differs greatly from one temperature of synthesis to the next one, observing a high polydispersity in all these Au systems. The growth behavior is modified when temperature changes, allowing the presence of one-dimensional structures, spheres and angular structures.

At 100 °C large particles were observed (~1 μm) in a variety of different well-defined geometric forms such as triangles, decahedrons, and truncated triangles, as observed in Figure 2a. Also rods with diameters between 50 and 150 nm and a few

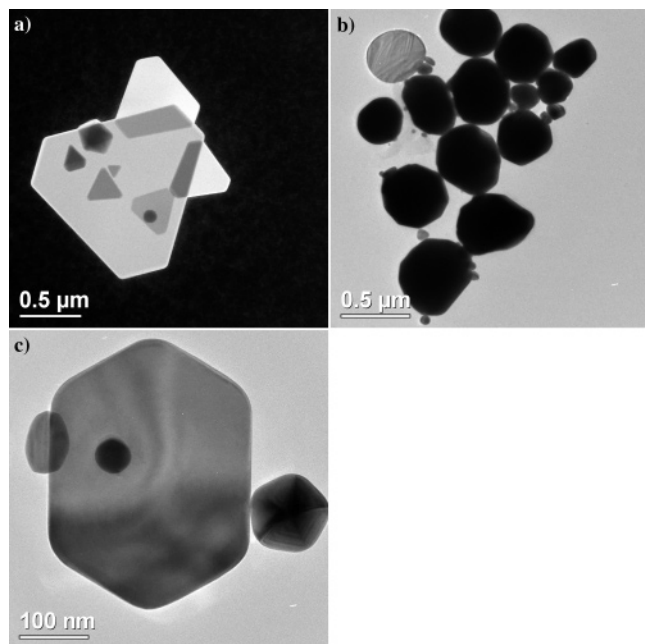


Figure 2. Analysis of Au particles (a) HAADF image of particles synthesized at 100 °C. Observe the well-defined geometrical shapes in the particles: triangles, truncated triangles and decahedrons. (b) TEM image of particles synthesized at 140 °C. It can be observed that the particles do not have a well-defined shape and tend to be more rounded. (c) TEM image of particles synthesized at 190 °C. Notice that the particles have better defined shapes than in the 140 °C case. The image shows the 2-dimensional projections of the particles with a hexagonal and a pentagonal shape.

micrometers in length were observed. All of these structures had very well-defined shapes. The final product was a clear solution with large Au precipitates, some of them visible to the bare eye.

At 140 °C more rounded particles were observed, with shapes less defined. These particles were also smaller (~500 nm) than in the 100 °C case. At this temperature the structures observed tend to be more spherical than in the previous case, as we can notice in Figure 2b. The final product at this temperature also was a clear solution with an evident precipitation of Au at the bottom of the flask.

Finally, at 190 °C the particles observed (~250 nm) were smaller than in the last two cases mentioned. At this temperature we can observe again particles with more geometric shapes than the ones observed at 140 °C, as we can see in Figure 2c. Some rods with less than 100 nm in diameter and less than 1 μm in length were observed. The final product at this temperature had a purple color with an observable precipitation of Au at the bottom of the flask.

Bimetallic Gold–Platinum Nanoparticles.

In the analysis of bimetallic systems, the reaction was studied under different temperatures observing the effect on the structure of the particles as a function of the rate of reduction and/or nucleation, size and dispersion. Also, the optical response of the samples on each reaction condition was analyzed.

Three different regimes were observed based on the temperature of reaction. Each regime showed nanoparticles with different structural and dimensional characteristics and optical responses. The results observed at the different temperatures are summarized in Table 1.

The first regime includes temperatures from 100 to 120 °C. Samples in this regime showed monometallic nanoparticles with a bimodal size distribution for the case of 100 and 110 °C; the smaller average size corresponds to the Pt nanoparticles, and the larger average size corresponds to the Au nanoparticles. The small Pt nanoparticles and the large Au particles observed are very similar to the ones in the monometallic case for the 100 °C case, as can be seen in Figure 3a. For the case of Au, some rods and other geometric shapes were detected. For 120 °C bimetallic nanoparticles started to appear and no bimodal distribution was observed.

The particles were determined to be monometallic from energy-dispersive spectroscopy (EDS) analysis. The analysis by UV–vis spectroscopy of the samples obtained at these three temperatures, showed a Au surface plasmon peak or a related feature. At 100 °C the peak is very clear; at 110 °C it is less intense, and at 120 °C it is almost non detectable and is slightly blue-shifted respect to the previous two, centered at approximately 510 nm. In Figure 4a we can observe a core–shell particle present in the 120 °C sample.

The second regime, from 130 to 170 °C, showed bimetallic nanoparticles with only one maximum in their size distribution and a small standard deviation. In this regime core–shell

TABLE 1: Results at Different Temperatures

T (°C)	average particle size (nm) \bar{X}	composition of particles	UV–vis peak	structure
100	$\bar{X}_1 = 4.72$ $\bar{X}_2 = 21.30$	Au and Pt monometallic	broad peak centered at ~520 nm	large Au particles, rods, triangles and pentagons. small Pt nanoparticles.
110	$\bar{X}_1 = 4.24$ $\bar{X}_2 = 27.52$	Au and Pt monometallic	broad peak centered at ~520 nm, less pronounced.	large Au particles without defined shape. small Pt nanoparticles
120	$\bar{X}_1 = 3.78$	Pt monometallic. Au–Pt: Au 50.92%, Pt 49.08% ^a	broad peak centered at ~510 nm, much less pronounced.	bimetallic nanoparticles, some core–shell. small Pt nanoparticles.
130	$\bar{X}_1 = 3.72$	Pt monometallic. Au–Pt: Au 45.8%, Pt 54.2% ^a	no detectable peak.	bimetallic nanoparticles, some core–shell. small Pt nanoparticles.
140	$\bar{X}_1 = 3.42$	Pt monometallic. Au–Pt: Au 48.49%, Pt 51.51% ^a	no detectable peak.	bimetallic nanoparticles, some core–shell. small Pt nanoparticles
150	$\bar{X}_1 = 4.13$	Pt monometallic. Au–Pt: Au 50.5%, Pt 49.5% ^a	no detectable peak.	bimetallic nanoparticles, some core–shell. small Pt nanoparticles
160	$\bar{X}_1 = 6.00$	Pt monometallic. Au–Pt: Au 55.6%, Pt 44.4% ^a	no detectable peak.	bimetallic nanoparticles, some core–shell. small Pt nanoparticles
170	$\bar{X}_1 = 6.68$	Pt monometallic. Au–Pt: Au 55.49%, Pt 44.51% ^a	no detectable peak.	bimetallic nanoparticles, some core–shell. small Pt nanoparticles
180	$\bar{X}_1 = 3.73$ $\bar{X}_2 = 7.77$	Pt monometallic. Au–Pt: Au 43.71%, Pt 56.29% ^a	broad feature centered at ~.510 nm. less intense.	bimetallic nanoparticles, some core–shell. small Pt nanoparticles
190	$\bar{X}_1 = 2.8$ $\bar{X}_2 = 6.6$	Pt monometallic. Au–Pt: Au 57.5%, Pt 42.5% ^a	broad peak centered at ~510 nm. less intense.	bimetallic nanoparticles some core–shell. small Pt nanoparticles

^a Twenty particles for each temperature were analyzed separately and the average of their composition is reported.

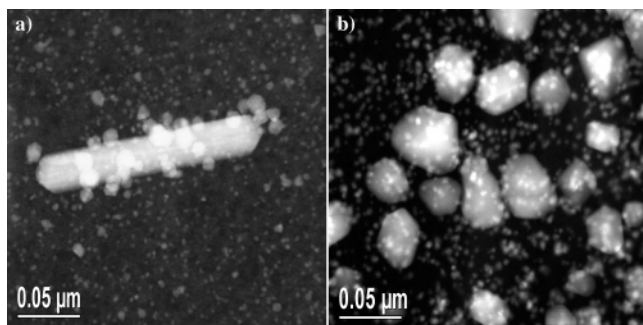


Figure 3. HAADF image of the Au–Pt system at the two first temperatures (a) at 100 °C (here we can observe larger particles (Au) with well-defined shapes and small particles (Pt) all over the image) and (b) at 110 °C (here the bimodal distribution in size is very clear). As in the last case, the larger particles correspond to the Au and the smaller ones correspond to the Pt.

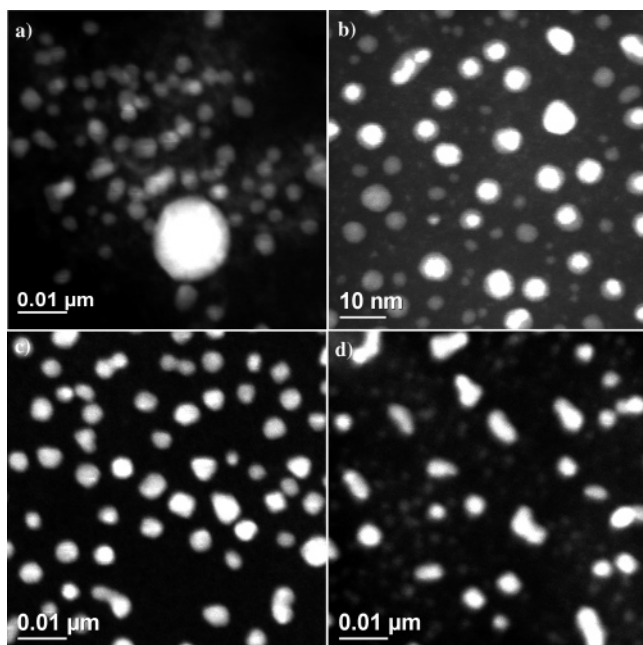


Figure 4. HAADF image of the Au–Pt nanoparticles system synthesized at different temperatures (a) at 120 °C (here we can observe a 16 nm particle which presents a clear brighter core and a less bright shell) and (b) at 140 °C (here the core–shell particles can be easily observed). At this temperature the smaller particle size and the smaller standard deviation were obtained (c) at 150 and (d) 160 °C.

structure can be observed in some of the particles, as seen in Figure 4b. At these temperatures no Au surface plasmon peak could be observed in the UV–vis spectra. Also, some Pt monometallic nanoparticles were detected in these samples.

The third and last regime includes the last two temperatures, 180 and 190 °C. At this reaction conditions, bimetallic nanoparticles were also present as in the previous regime, as observed in Figure 5. However, these structures were found more sparsely and also a bimodal size distribution was observed. In this case the smaller structures correspond to the Pt monometallic nanoparticles, which were found to be more abundant than in the last regime, while the larger ones correspond to the bimetallic nanoparticles. At these temperatures a Au surface plasmon feature can be observed again in the UV–vis spectra. The composition of the particles was determined by EDS in all the samples.

The analysis by UV–vis spectroscopy can be related to the structural conformation of the particles as observed by HAADF

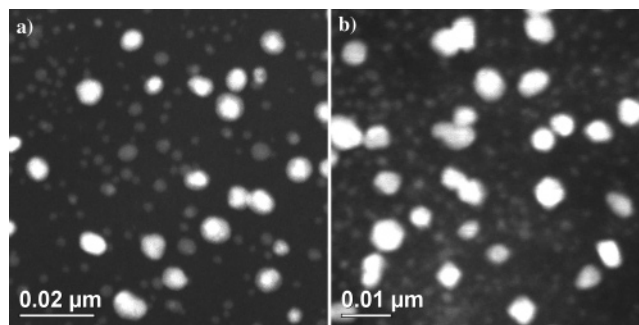


Figure 5. HAADF image of the Au–Pt system synthesized at the last two temperatures (a) at 180 °C (here the core–shell particles are clearly observed; these samples have a bimodal particle size distribution) and (b) at 190 °C. As in part a, samples at this temperature also present a bimodal particle size distribution

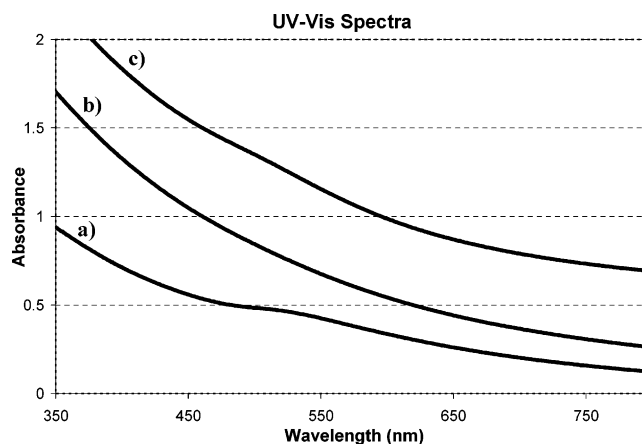


Figure 6. UV–vis spectrum of the Au–Pt system obtained (a) at 100 °C (the Au surface plasmon peak can be observed), (b) at 140 °C (here no peak or feature related to the Au optical response can be observed), and (c) at 190 °C (a broad feature related to the Au surface plasmon peak can be appreciated).

and the chemical composition. UV–vis spectra from the three different regimes are shown in Figure 6.

As can be observed from the UV–vis spectra, at lower temperatures the Au surface plasmon peak is well defined. This peak appears in the interval from 480 to 560 nm. But as the temperature of reaction increases, the peak starts to reduce its intensity until it reaches the temperatures of the second regime, where, as can be seen in Figure 6b, it becomes undetectable. Finally, as we get to the temperature of the third regime, a feature related to the Au surface plasmon peak start to be noticeable again, as presented in Figure 6c. For this last regime, no absorption peak was observed, but a barely noticeable shoulder can be appreciated between 470 and 560 nm.

The EXAFS and XANES results are presented next in the Discussion part of the work.

Discussion

Let's begin the discussion with the first regime (100 and 110 °C). As can be seen in Table 1, there is a marked tendency to form well-separated monometallic nanoparticles at the two temperatures of this regime. The analysis of HAADF images of these samples in Figure 3 show only particles with homogeneous contrasts. There were no identifiable changes in intensity that would indicate the presence of more than one type of element forming the particles. This hypothesis was supported with the results obtained with EDS. The optical response of these nanoparticles show an absorption peak localized in the

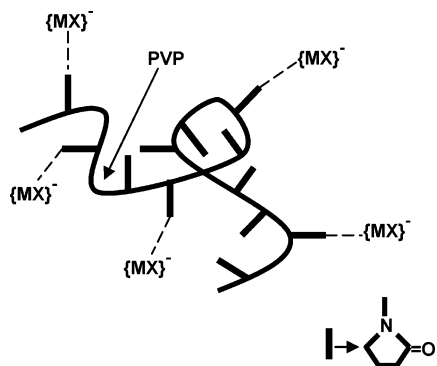


Figure 7. Schematic representation of the interaction between the PVP polymer chains and the metal precursor. M represents the metal and X the chlorine or the anionic species from the metallic precursor.

region between 480 and 560 nm as a wide band of low intensity. This band is reported as a characteristic band of Au nanoparticles with high polydispersity,⁴ also a deviation from the spherical shape in the nanoparticles can produce such a spectrum.²⁵ The Pt optical response does not appear in this region of the electromagnetic spectrum,^{26,27} and the UV–vis study was only based on the analysis of the Au surface plasmon peak. The bimodal distribution of sizes observed in Table 1 and in the HAADF images of Figure 3, the EDS analysis results, and the UV–vis spectra observed in this regime (Figure 6a) show that in the first regime we have a solution with a combination of Au and Pt monometallic nanoparticles.

As stated in reference,²⁸ Pt precursors tend to form stronger bonds than Au precursor with the C=O groups of the PVP (Figure 7), which can modify the reaction kinetics decreasing its rate of reduction. Along with this effect, platinum will be reduced in two stages, first to Pt²⁺ and then to Pt⁰, with a standard redox potential reported at room temperature of 0.775 V for [Pt⁴⁺Cl₆⁻]²⁻/[Pt²⁺Cl₄⁻]²⁻ and 0.68 V for [Pt²⁺Cl₄⁻]²⁻/Pt⁰. These two facts contribute to a lower generation of zero-valence Pt, in comparison with Au at the time of reduction. This means that the rate of reduction and nucleation of Pt under the studied conditions has a disadvantage toward the case of Au, for which a reported standard redox potential at room temperature is 1.002 V for [Au³⁺Cl₄]⁻/Au.^{7,8}

This disadvantage is more pronounced at lower temperatures, since at lower temperatures the oxidation potential of ethylene glycol is bigger than at higher temperatures.²⁹ This means that at lower temperatures the oxidation of ethylene glycol is less favored, which translates in fewer electrons available in the reaction environment to reduce the metals. As the temperature keeps increasing, the oxidation potential of the ethylene glycol decreases,²⁹ indicating that this electrochemical reaction is favored at higher temperatures. This translates as an increment in the electrons concentration in the reaction environment.

In contrast, the reduction potential of the metals is not affected by the temperature, according to F. Bonet et al.²⁹ It is insensitive to the reaction temperature, but there still is an effect on the reduction of the precursors related to the temperature dependence of the diffusion of metal species. Another effect of temperature on the reduction of the metal precursors is that the energy barrier that opposes to the reduction of the precursor is equal to the difference between the oxidation potential of the ethylene glycol and the reduction potential of the metal species. Once the oxidation potential of the ethylene glycol is lowered down to the same value of the reduction potential of the metal precursor, the reduction of the metal precursor will occur spontaneously and followed by the nucleation of metal nano-

particles.²⁹ From this analysis one can conclude that at higher temperatures the reduction of the metal species will be favored and also the oxidation of the ethylene glycol. This will decrease the time needed to reduce the metal precursor and the nucleation time needed to the formation of metal particles.

We believe that at these two lowest temperatures of the first regime (100 and 110 °C) the difference between the potential of Pt precursor reduction and the oxidation of the ethylene glycol is big enough to do not allow the Pt reduction and nucleation before the Au is added. But for the case of Au, the difference between its metal precursor reduction potential and the ethylene glycol oxidation potential is small enough to allow the reduction of the Au species to its zero valence state and to start the nucleation and growth processes of Au structures. When we add the Au to the reaction, the Pt precursor is still not reduced, and the Au starts to reduce and to nucleate, as just mentioned, and the Au monometallic structures that we observe in the HAADF images are produced. When the Pt finally reduces and starts to nucleate, a stronger interaction between the Pt precursor and the PVP could be the reason Pt and the Au did not form bimetallic structures at these temperatures. As stated by Ciacchi et al.,³⁰ Pt²⁺ ions have showed to form covalent bonds with some polymers, and act as a preferential site for nucleation of Pt clusters. In our study, the Pt clusters seem to prefer remain attached to the polymer, in our case PVP, rather than interact with the Au atoms. This leads to the formation of monometallic Au and Pt particles with the structural and optical characteristics mentioned before.

The particular case of 120 °C still is considerate as part of the first regime, mainly because we are still able to observe a small feature in the UV–vis spectra related to the Au surface plasmon peak and because we also observe particles bigger than 10 nm. In contrast to the monometallic particles detected in the first two temperatures, at this temperature we start to detect bimetallic nanoparticles.

HAADF images of bimetallic nanoparticles show contrast with different intensities in the same particle, as presented in Figure 4a. In this figure, a large nanoparticle with a core–shell structure surrounded by smaller nanoparticles can be observed. EDS analysis performed in these particles showed that the large core–shell nanoparticle was bimetallic with a higher concentration of Au than Pt, and the smaller nanoparticles were also bimetallic. These smaller bimetallic nanoparticles did not show a core–shell contrast in the HAADF images.

In the UV–vis spectrum for the sample presented in Figure 4a we observed that the wide, low intensity band due to gold decreases and has a blue shift; which can be an effect of the deposition of Pt onto the Au surface, this damps the surface plasmon peak of the gold, and the curve starts to flatten. For the case of particles around 16 nm, like the one observed in Figure 4a, the core size is around 12 nm and the shell has a thickness around 4 nm. In these cases the core must be formed mostly by Au, because it is much larger than any Pt nanoparticle observed in this study, and because of the higher concentration of Au in this specific kind of particles. For the case of the smaller bimetallic particles, which constitute most of this sample, the core–shell structure has been observed in very few cases.

We believe that 120 °C seems to be the temperature where the difference between the Pt precursor reduction potential and the potential of the ethylene glycol oxidation is small enough to allow the Pt species reduction and nucleation in a comparable rate with Au species, considering the extra minute that has been given to Pt in the reaction. This temperature value also seems to be when the interaction between Pt precursor and the PVP

becomes more instable and the increased mobility of the polymer eases the reduction of the Pt ions, increasing the coalitions of the zero-valence atoms which induce the formation of bimetallic nanoparticles. However, at this specific temperature we observe a combination of a few $\text{Au}_{\text{core}}\text{-Pt}_{\text{shell}}$ nanoparticles (particles > 10 nm) with smaller bimetallic nanoparticles that present the core-shell structure in a few cases. We got to these conclusions from the HAADF images, the EDS analysis results and the UV-vis spectroscopy analysis.

In the second regime, between 130 °C and 170 °C, no UV-visible absorption peak or feature was detected (Figure 6b), EDS analysis showed that the observed nanoparticles were bimetallic, no particle bigger than 10 nm were detected in any of the temperatures and the number of nanoparticles presenting the core-shell structure increased considerably, in comparison with the last temperature. All the samples synthesized at these different temperatures presented the just mentioned characteristics.

It is not an easy task to fully elucidate the entire features related to the core-shell structures. One analysis technique is not enough to obtain a complete insight of the elemental distribution and structure of the core-shell nanoparticles. Researchers have to use several characterization techniques combined to gain a better understanding of the core-shell particles. In our case, we use electron microscopy (HAADF), combined with UV-vis spectroscopy and X-ray absorption fine structure spectroscopy.

As we mention previously in the text, and as has been observed in the HAADF images presented for temperatures above 110 °C, a core-shell structure is commonly detected in some particles, with a brighter core and a less bright shell. We know from a previous work that this kind of core-shell contrast is attributed to core-shell nanoparticles.¹⁹ The source of this contrast, according to that work, is the strain field present in the interface between core and shell, due to the difference in their lattice constant produced by the difference in compositions.

Then we tried to determine which element was located in the core and which one in the shell. As a first approximation we proposed a $\text{Au}_{\text{core}}\text{-Pt}_{\text{shell}}$ structure. On the basis of previous works reported by several authors,^{3,4,7,8,12,13,20,21,31,32} we proposed that the deposition of a Pt shell on top of a Au core will be responsible for the disappearance of the Au surface plasmon peak on the UV-vis absorption spectrum. It has been reported that the deposition of one metal on the other can produce damping of the surface plasmon peak related to the metal where the second one is depositing; this has been reported not only for the Au-Pt system but also for the Au-Pd, Au-Cu, and Ag-Co. We wanted to compare our results with theoretical ones calculated by means of Mie theory for coated particles, as has been done by several authors in other related works.^{3,4,9,12} From ref 4 we obtained the expression to calculate the spectra of core-shell nanoparticles and the optical constants from refs 33 and 34. For this model we also need the volume fraction of the shell layer, g . For $g = 0$ we have the same case of a particle made only from the element present in the core, and for $g = 1$ it is the same case as if we have a particle made only from the element present in the shell. We will obtain this parameter g from our experimental HAADF images. The calculated spectra for several values of g and for the two possible cases, $\text{Au}_{\text{core}}\text{-Pt}_{\text{shell}}$ and $\text{Pt}_{\text{core}}\text{-Au}_{\text{shell}}$ are shown in Figure 8.

Our results for the calculated UV-vis absorption spectra were in great accordance with those reported by L. M. Liz-Marzan and A. P. Philipse.⁹ In their work they calculated the UV-vis spectra for both cases $\text{Au}_{\text{core}}\text{-Pt}_{\text{shell}}$ and $\text{Pt}_{\text{core}}\text{-Au}_{\text{shell}}$. They

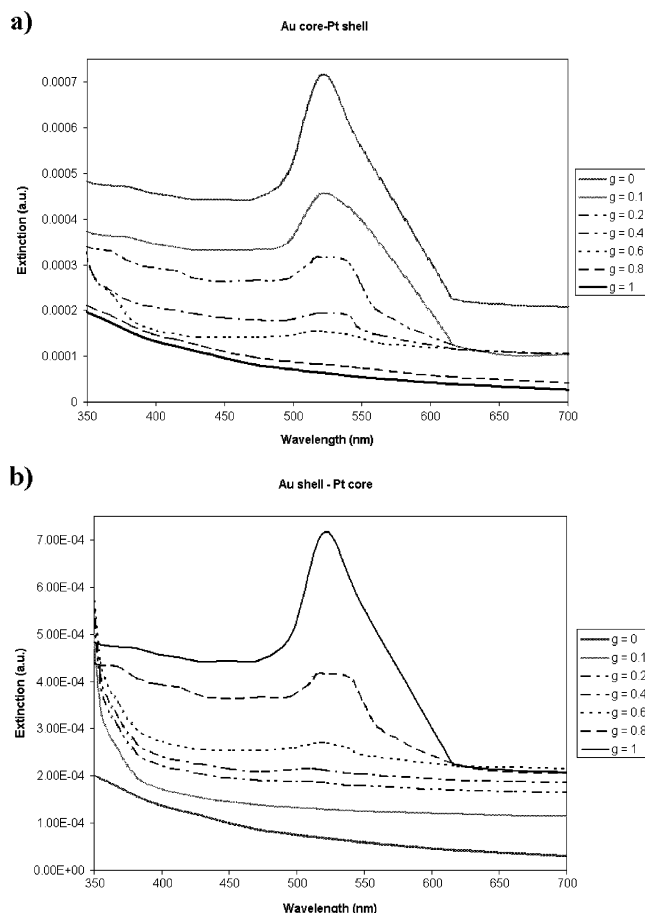


Figure 8. Calculated spectra for a coated spherical particle for different values of g . (a) For the $\text{Au}_{\text{core}}\text{-Pt}_{\text{shell}}$ case and (b) for the $\text{Pt}_{\text{core}}\text{-Au}_{\text{shell}}$ case (offsets for clarity).

calculated the volume fraction of the core and the shell based in their initial Au and Pt concentrations to calculate the UV-vis spectra. They also observed an increment and a red shift in the Au surface plasmon peak for the $\text{Pt}_{\text{core}}\text{-Au}_{\text{shell}}$ case as the Au shell thickness increased and a decrement with a blue shift in the Au surface plasmon peak for the $\text{Au}_{\text{core}}\text{-Pt}_{\text{shell}}$ case as the Pt shell increased.

We obtained the average particle size and the g value from our experimental images. For the sample synthesized at 140 °C, we measured an average g value of 0.29. And for the 180 °C and 190 °C temperatures we obtained an average g value of 0.45. If we compare our experimental spectra from Figure 6 with the calculated ones, based on the amplitude of the UV-vis absorption peak and the g values obtained from our samples, we concluded that the $\text{Pt}_{\text{core}}\text{-Au}_{\text{shell}}$ spectra describe in a more accurate way our experimental results.

To obtain additional information on the metals interaction in the bimetallic nanoparticles and the nature of the core and the shell, we performed a number of synchrotron X-ray absorption studies on the samples of Pt monometallic nanoparticles and the bimetallic nanoparticles synthesized at 140 °C. Figures 9 and 10 compare the normalized Pt L_3 and L_2 -edges XANES spectra for the Pt monometallic nanoparticles and for the bimetallic nanoparticles synthesized at 140 °C with those for the bulk Pt. The difference spectra are also presented in order to give emphasis to the variations in the white line intensity between the mono and bimetallic samples respect to the Pt bulk system. The observed changes in Figure 9 for the monometallic sample have been already shown, both theoretically and experimentally for bare Pt nanoclusters and Pt supported ones,

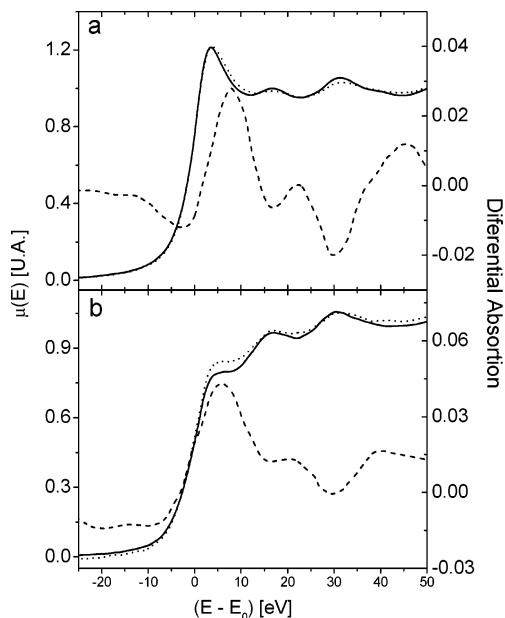


Figure 9. Comparison between the absorption L₃ (a) and L₂ (b) edges of Pt nanoparticles (dotted line) and bulk Pt (solid line). Dashed lines show the difference spectra between nanoparticles and bulk Pt samples.

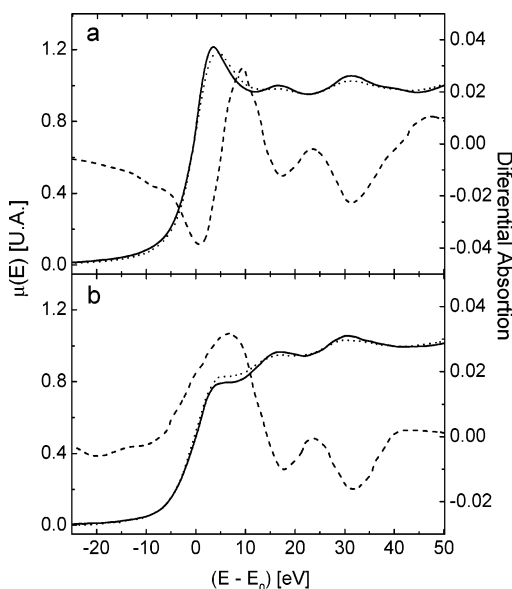


Figure 10. Comparison between the absorption L₃ (a) and L₂ (b) edges of bimetallic sample synthesized at 140 °C (dotted line) and bulk Pt (solid line). Dashed lines show the difference spectra between bimetallic AuPt nanoparticles and Pt-bulk samples.

respectively,^{35,36} for small Pt clusters and are exclusively ascribed to size effects.

It is well-known that the formation of Pt-metal bonds modifies the chemical properties of Pt.³⁷ There are also electronic perturbations induced by alloy formation,^{38–43} evidenced in the white line intensity. In our case, these changes are not observed in the bimetallic clusters (see Figure 10) and the small differences between the sample's and the Pt foil L₃ profiles can be ascribed in principle only to size effects as in the monometallic sample.

This qualitative observation at the difference L_{2,3} XANES spectrum, between samples and Pt-bulk reference, can be quantitatively confirmed by determining the change in the number of 5-d holes in the bimetallic system for the platinum atoms using a variation of the method described by Mansour et

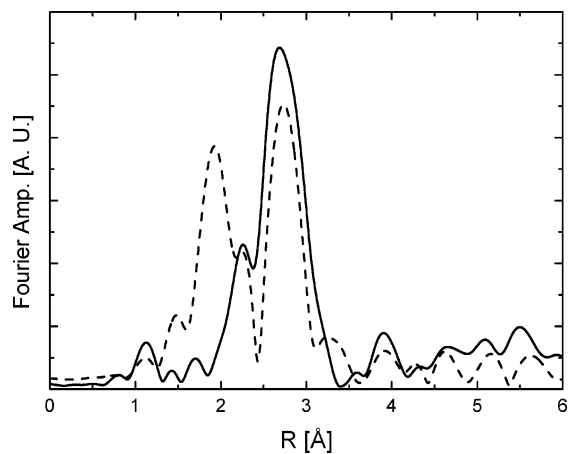


Figure 11. Comparison of the radial distribution functions of the Au foil (solid line) and the bimetallic system synthesized at 140 °C (dashed line), in the Au L₃ edge. The bimetallic system was measured at 20 K. The Au foil Fourier amplitude was divided by 5 for scaling purposes.

TABLE 2: Fractional Change in the Total Number of Unfilled States in the d Band Compared to the Number in the Platinum Foil (f_d) and the Number of Unfilled d States in the Samples (h_{Ts}) for Pt Nanoparticles and Bimetallic System Synthesized at 140 °C

sample	f_d	h_{Ts}
Pt nanoparticles (140 °C)	0.0148	1.624
Pt–Au (140 °C)	0.0089	1.614

al.^{38,39} As it can be seen from Table 2, the variation in the number of 5-d holes of the bimetallic sample synthesized at 140 °C is of the same order of magnitude of the monometallic system.

The trend observed for the Pt XANES L-edges spectra is also observed when analyzing Au L₂ and L₃ XANES spectra, but as no white line is present in Au L₃-edge spectrum, the differences are even smaller and difficult to quantify.

Obtained XANES results on Pt and Au L-edges show, in summary, that there is no electronic transfer between Au and Pt, this would constitute an indirect evidence that the elements are segregated from each other and are not forming an alloy.

Figure 11 shows the radial distribution function of Au (without phase correction) for the bimetallic sample synthesized at 140 °C, obtained from the Au-L₃ EXAFS spectrum. These EXAFS data lets us identify which of the elements are in the shell in the bimetallic nanoparticles. This identification is based on the presence of a contribution in the radial distribution function of Au in the range of 1–2 Å. These contributions are the typical bond distances for low Z elements such as O, N, and C, which are present in the PVP. An analysis of the amplitude and phase of this contribution confirms that this low R contribution in the radial distribution function of Au is due to low Z scatters.

In contrast, such contribution is not observed in the radial distribution function of Pt atoms as it is shown in Figure 12. The comparison with the bulk Pt shows that in the surroundings of Pt atoms only Pt atoms are found and there is no evidence of any low Z scatters.

All these results support the idea of a core–shell structure for the temperatures of the second regime, where the core is made from Pt and the shell is made from Au, segregated from each other. For the case of the particles that do not present the core–shell structure, an eutectic alloy is proposed, where both elements are present in the particle, but segregated from each other in a different way from the core–shell. From these results

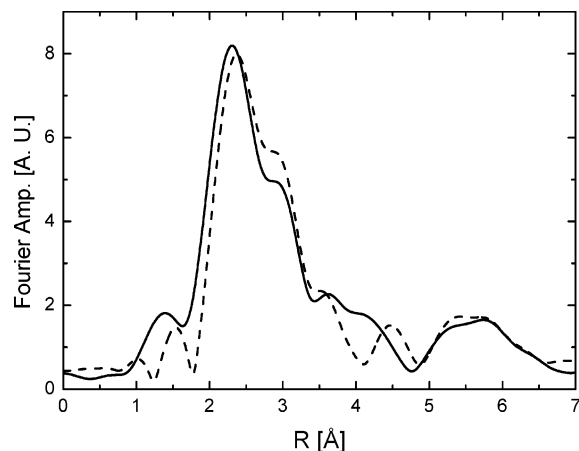


Figure 12. Comparison of the radial distribution functions of the Pt foil (solid line) and the bimetallic system synthesized at 140 °C (dashed line), in the Pt L_3 edge. The bimetallic system was measure at 20 K. The Pt foil Fourier amplitude was divided by 5 for scaling purposes.

we cannot rule out that there could be a small fraction of particles where the elements do form an alloy or Pt interacts with PVP, because we must have in mind that EXAFS and XANES gives us average information of the analyzed sample. The analysis and interpretation of the rest of the data obtained from the XANES and EXAFS studies are still under progress and is intended for another work.

From the arguments just presented, we believe that in the temperatures of the second regime (130–170 °C), due to the difference between the Pt precursor reduction potential and the ethylene glycol oxidation potential, the Pt reduction and nucleation take place in the minute before the Au is added to the reaction. When Au is added, it starts to reduce and to deposit onto the already formed Pt cores and subsequently forms the Au shells. We believe this is the mechanism of formation of the observed bimetallic core–shell nanoparticles.

Finally, in the third regime (180 and 190 °C) we observe again a bimodal distribution, where the smaller average size corresponds to Pt monometallic nanoparticles and the bigger average size corresponds to bimetallic nanoparticles, as determined from EDS analysis. At these temperatures we can observe some particles with the core–shell structure. The UV–vis spectra for these temperatures show a low intensity broad shoulder centered at approximately 510 nm, as observed in Figure 6c. We believe that the rate of reduction and nucleation of the Pt is even higher than in the last temperature regime, which again will allow the formation of the Pt cores where subsequently the Au atoms are going to deposit and form the shell. The reason we are able to see a feature related to the Au surface plasmon peak at these higher temperatures is related to the thicker shells observed in the HAADF images for these samples. This appearance of a low intensity feature centered at approximately 510 nm on the UV–vis spectrum is also consistent with the calculated spectra for the $Pt_{core}-Au_{shell}$ case, as the Au shell increases its thickness.

At the same time the core–shell structures are produced, eutectic alloyed nanoparticles, not core–shell structures, are formed by the coalitions among atoms for all the temperatures where bimetallic nanoparticles were detected, since this kind of nanoparticles was observed in all the temperatures studied.

The optimum temperature to prepare well-dispersed nanoparticles, with a narrow size distribution, the smallest average particle size, and the most core–shell structures, was 140 °C. HAADF image on Figure 4b shows some structures with two well-defined intensities and some of them with no apparent

difference; however, the elemental chemical composition of both structures are Au and Pt. In a previous work,¹⁹ it was mentioned that core–shell contrast depends on the orientation of the particle with respect of the electron beam in the TEM. On the basis of this argument, we performed some tilting experiments in particles that did not show core–shell contrast, like some of the particles observed in Figure 4. Some particles showed core–shell contrast after a few degrees of tilting, but there were other particles that, even after tilting the sample at different angles, never presented core–shell contrast,¹⁹ which suggests us that this could be eutectic alloyed bimetallic nanoparticles. The same conclusion was obtained for the particles with homogeneous contrast observed in the rest HAADF images of Figure 4.

Au and Pt have atomic numbers of 79 and 78, respectively. Seeing the difference between Au and Pt in a HAADF images would be very difficult, because one of the most important factors determining the intensity observed by this technique is the atomic number, even though we should be able to observe the interface between the Au and the Pt in the eutectic alloyed nanoparticles, just like in the core–shell structure. But so far we have not observed a good example of these particles where we can see the interface between Au and Pt in a different way from the core–shell. We think the fact that these interfaces are a not 3-dimensional structure, like the core–shell case, makes them more difficult to observed by this technique, specially since the contrast produced by this interfaces depends on the orientation of the nanoparticle with respect of the electron beam. Another reason is that these interfaces would be more like line defects smaller than the electron probe size, which is responsible for the HAADF technique resolution.

For our results at 120 °C, a more detailed analysis is necessary, since at this temperature the nanoparticles presented very different characteristics compared to the ones obtained at other temperatures. EXAFS and XANES studies are intended to help in the elucidation of the structures and elemental distribution of the nanoparticles observed at this temperature.

With respect to the monometallic cases, Pt did not show important variations as the temperature was increased, neither in size nor in structure. This fact has been already reported by Bonet et al.¹⁶ We can observe how the core sizes and shapes for the bimetallic core–shell nanoparticles are pretty similar to the sizes and shapes observed in the Pt monometallic nanoparticles. For the case of Au, coordination with PVP plays an important role in the nucleation and growth of Au nanostructures. Figure 2 shows different types of particles obtained at 100, 140, and 190 °C. And from these images we can conclude that at lower temperatures we have larger particles. One possible explanation for this phenomenon is that at lower temperatures, nucleation and growth take place at the same time, leading to the formation of both large particles and new nuclei, as stated by Silvert and Tekaija-Elhsissen.⁴⁶ However, as the temperature increases the particle size decreases, it is well-known that at higher temperatures the formation of metallic nuclei is more favorable, having more seeds to create nucleation sites, resulting in the decreasing particle size and in an increment in the number of particles.⁴⁶

Conclusions

From this study it was found that the temperature plays a decisive role in the synthesis of bimetallic Au–Pt nanoparticles protected with PVP by the polyol method. It does not only affect the rates of reduction and nucleation of the metals, but it also affects the coordination between the metals and the polymeric protective agent, the distribution of elements in the nanoparticles, and the final particle size.

The analysis of the bimetallic synthesis suggests that at lower temperatures (100 °C and 110 °C) the Au reduces and nucleates much faster than the Pt and that an interaction between Pt and PVP is strong enough to prevent the two elements from forming bimetallic structures, as explained earlier. However, at 120 °C there seems to be a balance between the reduction and nucleation rates of Pt and Au, considering Pt was given one more minute in the reaction. This is why we observe an interaction between the elements and the formation of bimetallic structures. However, at this temperature there is a combination of a few Au_{core}–Pt_{shell} nanoparticles (particles > 10 nm) with a combination of Pt_{core}–Au_{shell} nanoparticles (particles < 10 nm) and eutectic alloyed nanoparticles. In the temperature range between 130 and 170 °C, Pt_{core}–Au_{shell} particles were obtained. And in the last two temperatures (180 and 190 °C), Pt_{core}–Au_{shell} nanoparticles with thicker Au shells were synthesized, as observed in the HAADF images. In all the temperatures above 110 °C, the presence of eutectic alloyed nanoparticles was detected by the tilting experiment mentioned above.

We have presented here a detailed analysis by UV–vis spectroscopy, electron microscopy, and X-ray absorption techniques of the types of metallic nanoparticles obtained by the polyol method showing the importance of the temperature control in the synthesis in order to accomplish monometallic and bimetallic nanoparticles with the desired optical, dimensional and structural characteristics. We have also demonstrated that the combination of these three techniques makes a novel tool for the full understanding of core–shell structures in combination with calculated UV–vis absorption spectra; and how the use of only one technique to study core–shell nanoparticles is not sufficient to obtain a full understanding of the system.

Acknowledgment. The authors will like to thank the support received from the Merck foundation; and the Reese Chair of Engineering from the Chemical Engineering Department of the University of Texas at Austin. We also will like to thank the Texas Materials Institute in the University of Texas at Austin. D.G.G. wants to acknowledge the support received from CONACYT Mexico and wishes to thank Jose Luis Elechiguerra for valuable discussions. We also thank CONICET and the Fundación Antorchas (Argentina) and the LNLS (Brazil) under Projects D04-XAS1 2802/04 and 2317/03.

References and Notes

- Thomas, J. M.; Raja, R.; Johnson, B. F. G.; Hermans, S.; Jones, M. D.; Khimyak, T. *Ind. Eng. Chem. Res.* **2003**, *42*, 1563.
- Bronstein, L. M.; Chernyshov, D. M.; Volkov, I. O.; Ezernitskaya, M. G.; Valetsky, P. M.; Matveeva, V. G.; Sulman, E. M. *J. Catal.* **2000**, *196*, 302.
- Mulvaney, P.; Giersig, M.; Henglein, A. *J. Phys. Chem.* **1992**, *96*, 10419.
- Mulvaney, P. *Langmuir* **1996**, *12*, 788.
- Chushak, Y. G.; Bartell, L. S. *J. Phys. Chem. B* **2003**, *107*, 3747.
- Wu, M. L.; Chen, D. H.; Huang, T. C. *Langmuir* **2001**, *17*, 3877.
- Wu, M. L.; Chen, D. H.; Huang, T. C. *Chem. Mater.* **2001**, *13*, 599.
- Yonezawa, T.; Tushima, N. *J. Mol. Catal.* **1993**, *83*, 167.
- Liz-Marzan, L. M.; Philipse, A. P. *J. Phys. Chem.* **1995**, *99*, 15120.
- Han, S. W.; Kim, Y.; Kim, K. *J. Colloid Interface Sci.* **1998**, *208*, 272.
- Schmid, G. *Clusters and Colloids, From theory to Applications*; VCH Publishers: Weinheim, Germany, 1994.
- Kan, C.; Cai, W.; Li, C.; Zhang, L.; Hofmesiter, H. *J. Phys. D: Appl. Phys.* **2003**, *36*, 1609.
- Sanchez-Ramirez, J. F.; Pal, U. *Superficies Vac.* **2001**, *13*, 114.
- Viau, G.; Toneguzzo, P.; Pierrard, A.; Acher, O.; Fievet-Vincent, F.; Fievet, F. *Scripta Mater.* **2001**, *44*, 2263.
- Tekaia-Elhsissen, K.; Bonet, F.; Silvert, P. T.; Herrera-Urbina, R. *J. Alloys Compounds* **1999**, *292*, 96.
- Bonet, F.; Delmas, V.; Grugeon, S.; Herrera-Urbina, R.; Silvert, P. Y.; Tekaia-Elhsissen, K. *NanoStruct. Materials.* **1999**, *11*, 1277.
- Turkevich, J.; Stevenson, P.; Hillier, J. *Discuss. Faraday Soc.* **1951**, *11*, 55.
- Tsen, S.-C. Y.; Crozier, P. A.; Liu, J. *Ultramicroscopy* **2003**, *98*, p 63.
- Garcia-Gutierrez, D.; Gutierrez-Wing, C.; Miki-Yoshida, M.; Jose-Yacamán, M. *Appl. Phys. A* **2004**, *79*, p 481.
- Alvarez, M. M.; Khoury, J. T.; Schaaff, G.; Shafiqullin, M. N.; Vezmar, I.; Whetten, R. L. *J. Phys. Chem. B* **1997**, *101*, 3706.
- Henglein, A. *J. Phys. Chem. B* **2000**, *104*, 2201.
- Carotenuto, G.; Pepe, G. P.; Nicolais, L. *Eur. Phys. J. B* **2000**, *16*, 11.
- Sun, Y.; Yin, Y.; Mayers, B. T.; Herricks, T.; Xia, Y. *Chem. Mater.* **2002**, *14*, 4736.
- Bonet, F.; Tekaia-Elhsissen, K.; Sarathy, K. V. *Bull. Mater. Sci.* **2000**, *23*, 165.
- Yu, Y. Y.; Chang, S. S.; Lee, C. L.; Wang, C. R. *J. Phys. Chem. B* **1997**, *34*, 6661.
- Qu, S.; Song, Y.; Liu, H.; Wang, Y.; Gao, Y.; Liu, S.; Zhang, X.; Li, Y.; Zhu, D. *Optics Commun.* **2002**, *203*, 283.
- Mafune, F.; Kohno, J.; Takeda, Y.; Kondow, T. *J. Phys. Chem. B* **2003**, *107*, 4218.
- Sugimoto, T. *Fine Particles Synthesis, Characterization, and Mechanisms of Growth*; Surfactant Series Vol. 92; Marcel Dekker: Basel, 2000.
- Bonet, F.; Guery, C.; Guyomard, D.; Herrera-Urbina, R.; Tekaia-Elhsissen, K.; Tarascon, J. M. *Int. J. of Inorg. Mater.* **1999**, *1*, 47.
- Ciacchi, L. C.; Mertig, M.; Pompe, W.; Meriani, S.; De Vita, A. *Platinum Metals Rev.* **2003**, *47*, 98.
- Sobal, N. S.; Hilgendorff, M.; Mohwald, H.; Giersig, M.; Spasova, M.; Radetic, T.; Farle, M. *Nano Lett.* **2002**, *2* (6), 621.
- Pal, U.; Sanchez Ramirez, J. F.; Liu, H. B.; Medina, A.; Ascencio, J. A. *Appl. Phys. A* **2004**, *79*, p 79.
- (a) Johnson, P. B.; Christy, R. W. *Phys. Rev. B* **1972**, *6*, 4370. (b) Weaver, J. H.; Krafska, C.; Lynch, D. W.; Koch, E. E. *Optical Properties of Metals: Physics Data Series 18–2*; Fachinformationszentrum Karlsruhe: 1981; Vol. 2.
- (a) Weaver, J. H. *Phys. Rev. B* **1975**, *11*, 1416. (b) Weaver, J. H.; Krafska, C.; Lynch, D. W.; Koch, E. E. *Optical Properties of Metals: Physics Data Series 18–2*; Fachinformationszentrum Karlsruhe: 1981; Vol. 1
- Bazin, D.; Sayers, D.; Rehr, J. J.; Mottet, C. *J. Phys. Chem. B* **1997**, *101*, 5332.
- Ankudinov, A. L.; Rehr, J. J.; Low, J. J.; Bare, S. R. *Topics Catal.* **2002**, *18*, 3.
- Rodriguez, J. A.; Jirsak, T.; Chaturvedi, S.; Hrbek, J. *J. Am. Chem. Soc.* **1998**, *120*, 11149.
- Santori, G.; Casella, M.; Ferretti, O.; Ramallo-López, J. M.; Giovanetti, L.; Requejo, F. G. *J. Phys. Chem. B* **2003**, *107* (41), 1144.
- Stagg, S. M.; Querini, C. A.; Alvarez, W. E.; Resasco, D. E. *J. Catal.* **1997**, *168*, 75.
- Jeon, Y.; Chen, J.; Croft, M. *Phys. Rev. B* **1994**, *50*, 6555.
- Borgna, A.; Garetto, T. F.; Apesteguía, C. R.; Moraweck, B. *Appl. Catal. A: Gen.* **1999**, *182*, 189.
- Viswanathan, R.; Liu, R.; Smotkin, E. S. *Rev. Sci. Instrum.* **2002**, *73*, 2124.
- Hill E. K.; Baudoing-Savois, R.; Moraweck, B.; Renouprez, A. *J. Phys. Chem.* **1996**, *100*, 3102.
- Mansour A. N.; Cook, J. W.; Sayers D. E. *J. Phys. Chem.* **1984**, *88*, 2330.
- Reifsnnyder, S. N.; Otten, M. M.; Sayers, D. E.; Lamb, H. H. *J. Phys. Chem. B* **1997**, *101*, 4972.
- Silvert, P. Y.; Tekaia-Elhsissen, K. *Solid State Ionics* **1995**, *82*, 53.